



# Multifunctional microcapsules based on ZnO and n-octadecane: From thermal energy storage to photocatalytic activity

Javier Sánchez-Fernández, Teresa Aguilar, Ivan Carrillo-Berdugo, Juan Jesús Gallardo, Javier Navas\*

Departamento de Química Física, Facultad de Ciencias, Universidad de Cádiz, E-11510, Puerto Real, Cádiz, Spain

## HIGHLIGHTS

- Microcapsules based on ZnO containing C18 as phase change material were synthesized.
- These microcapsules in buildings will increase the amount of sensible heat stored.
- The microcapsules are also stable after heating/cooling cycles.
- ZnO and C18-based microcapsules show photocatalytic activity.
- The microcapsules can be used to remove organic pollutants from buildings.

## ARTICLE INFO

### Keywords:

Energy materials  
Thermal properties  
Microcapsules  
Phase change materials

## ABSTRACT

Energy management is one of the most important issues to be addressed in the near future in many fields, one of which is buildings. In this sense, new phase change materials (PCM) are being widely studied for storing energy. Encapsulating PCM is a good way to incorporate these materials into different applications in which energy storage is useful. In this study, microcapsules based on ZnO containing n-octadecane as a phase change material were synthesized and characterized with regard to their structural, morphological and optical properties according to several synthesis parameters, such as the proportion of precursors, stirring rate and ageing time. The microcapsules were characterized using x-ray diffraction, Fourier transform infrared spectroscopy, scanning electron microscopy, and UV-Vis spectroscopy in diffuse reflectance mode. The presence of n-octadecane inside the capsules was confirmed. Their thermal behaviour was analysed by means of differential scanning calorimetry. Heating/cooling cycles were performed, after which the microcapsules presented good stability. Furthermore, the encapsulation efficiency was estimated from melting and crystallization enthalpy values, reaching a value of 23.1%. Moreover, the isobaric specific heat of the microcapsules is higher than that of ZnO, which means that substituting ZnO with microcapsules in buildings leads to an important increase in the amount of sensible heat stored. Finally, the photocatalytic activity of the microcapsules was analysed by studying the photo-degradation of Crystal Violet dye. The degradation rate increased when the microcapsules were present, so the photocatalytic activity of the microcapsules was confirmed under UV and visible irradiation, which is of interest because they can be used to remove organic pollutants from buildings.

## 1. Introduction

Today, the energy crisis, the increase in pollution, and climate change are important problems that our society must attempt to resolve in the very near future. Energy consumption in the world continues to grow, which leads to a very high use of fossil fuels, the largest sources of CO<sub>2</sub> emissions. In this sense, researchers from all over the world are

working on the development of new methods for the production, conversion and storage of energy. In recent decades, different renewable energy sources have been studied for the production of energy, but they present problems in terms of their implementation due to their intermittency. Consequently, different energy storage technologies are under study. For example, the Power-to-X (P2X) methods are being studied for their potential to create long term storage possibilities. They can replace

\* Corresponding author.

E-mail address: [javier.navas@uca.es](mailto:javier.navas@uca.es) (J. Navas).

<https://doi.org/10.1016/j.matchemphys.2023.127501>

Received 22 September 2022; Received in revised form 31 January 2023; Accepted 12 February 2023

Available online 16 February 2023

0254-0584/© 2023 Elsevier B.V. All rights reserved.

fossil fuels with H<sub>2</sub> and CH<sub>4</sub> or other useful chemicals, and become part of the future energy solution [1]. Another option that is attracting considerable attention from many researchers is the use of phase change materials (PCM) for thermal energy storage. These materials are capable of storing energy as latent heat in their own bonds [2]. They are being tested for various applications such as solar heating systems [3], domestic cooling/heating [4] or in concentrating solar systems for direct steam production [5].

PCMs can also be used in building materials since they are capable of capturing and supplying large amounts of energy during melting and solidification processes at specific temperatures [6]. For this application it is necessary to consider what the phase change of the material is and at what temperature takes place. Phase changes can be liquid-gas, solid-gas, solid-solid, or solid-liquid. The application in construction materials of those that involve a gas phase is complicated due to the changes in volume and pressure that these phase changes will generate. On the other hand, solid-solid changes usually imply lower stored energy values than in other cases. For these reasons, PCMs involving solid-liquid transition are the most extended in building materials.

Paraffins [7] and fatty acids [8] are PCMs that generate this phase change and show interesting properties, such as the temperature at which the phase change occurs, as well as the energy that they are capable of storing as latent heat. However, their use presents various problems, such as in some cases their flammability, but also because it is limited by presenting a liquid phase. These problems can be solved by encapsulation processes [6], whereby the PCM (core) is covered by a protective material (shell). This material must present good mechanical properties and thermal conductivity so that the PCM remains stable inside the shell. In this sense, several materials have been proposed for encapsulating PCMs, such as SiO<sub>2</sub> [9], TiO<sub>2</sub> [10], Al<sub>2</sub>O<sub>3</sub> [11], CuO [12], or C-based materials [13]. Table 1 shows some key findings on this topic.

Therefore, in this work, n-octadecane (C18) is encapsulated using ZnO, selected because of its interesting properties, such as its low toxicity and the fact that it is a semiconductor with piezoelectric [18], optoelectronic [19] and photocatalytic [20–22] properties. In addition, the control of the intrinsic defect structures in ZnO nanostructures leads to the design of appealing materials for several applications such as in supercapacitor devices [23–27]. Mg doping makes it possible to control the optical band gap of ZnO [28,29], while Al doping leads to ZnO thin films with appealing structural and optical characteristics [30]. Therefore, ZnO is a promising material for different applications. However, the use of ZnO for designing multifunctional microcapsules with applications in thermal energy storage and photocatalysis is really new. The physical and chemical properties of the microcapsules were characterized using several techniques such as x-ray diffraction, scanning electron microscopy, Fourier transform infrared spectroscopy and UV–vis spectroscopy in diffuse reflectance mode. To analyse the possible

applications of the microcapsules synthesized, their thermal behaviour was analysed using a differential scanning calorimetry technique to obtain the melting and crystallization enthalpies. Moreover, their isobaric specific heat was measured. Finally, as ZnO shows semiconductor behaviour, the photocatalytic activity of the microcapsules synthesized was analysed by the photodegradation of crystal violet dye.

## 2. Experimental

### 2.1. Reagents

Sigma-Aldrich® supplied n-octadecane (C18, purity ~ 99%), hexadecyltrimethylammonium bromide (CTAB, purity ≥99%), zinc sulphate heptahydrate (ZnSO<sub>4</sub>·7H<sub>2</sub>O, purity ≥99%). Sodium hydroxide (NaOH, purity ≥99%) was supplied by Probus®.

### 2.2. Synthesis of microcapsules

The ZnO capsules with a C18 core were synthesized following the precipitation method reported by Li et al. [31]. First, an emulsion of C18 and water was prepared by vigorous stirring at 60 °C for 90 min, adding 2.33g of CTAB, a surfactant with amphipathic properties. The methyl groups of CTAB interact with C18 while polar groups interact with water molecules, forming a homogeneous emulsion. The amount of C18 was modified to change the C18/ZnSO<sub>4</sub> ratio, as described below, using 2.4 g and 2.6 g of C18. CTAB and C18 was added to 50 mL of water, resulting in a C18:water ratio of about 1:20. Next, ZnSO<sub>4</sub> was diluted in 30 mL of water, and added dropwise (2.5 mL/min) to the emulsion as a source of Zn<sup>2+</sup> ions under stirring at 60 °C for 4 h. The Zn<sup>2+</sup> are placed close to the polar groups of CTAB surrounding the C18 drops. Then, a 1 M solution of NaOH was added dropwise (1 mL/min) under stirring at 60 °C for 6 h to obtain a pH = 11. NaOH is a source of OH<sup>-</sup> ions, which react with Zn<sup>2+</sup> to obtain Zn(OH)<sub>2</sub> and ZnO. Both compounds can be formed at pH = 11. Then, an ageing process took place at 85 °C without stirring, which favours the transformation of Zn(OH)<sub>2</sub> to ZnO according to [32].



Finally, the C18@ZnO microcapsules were obtained after filtration, and then they were washed five times using 25 mL of water at 40 °C. A white solid was obtained and dried at 40 °C for 24 h.

In order to optimise the conditions for obtaining the best microcapsules, three parameters were analysed. First, the ratio of C18 and ZnSO<sub>4</sub>. Typically, other capsules have been prepared using a 50:50 ratio, but we also tested a 60:40 ratio. The stirring rate was also tested. We

**Table 1**

A summary of key findings from a literature review.

PCM/Core	Shell	Key findings	Ref.
Paraffin	SiO <sub>2</sub>	Encapsulation ratio of 78%, and latent heat about 156 J g <sup>-1</sup>	[7]
Palmitic acid	PAMA <sup>a</sup>	Good thermal reliability after 100 cycles	[8]
n-octadecane	SiO <sub>2</sub>	A new self-assembly synthesis for silica encapsulation. Good stability after 100 cycles	[9]
Mystiric acid	TiO <sub>2</sub>	Good thermal stability and higher latent heat	[10]
Al <sub>2</sub> O <sub>3</sub>	Al	Application temperature about 600 °C	[11]
C22	GO-CNT <sup>b</sup>	Excellent stability	[12]
Paraffin	UF <sup>c</sup> with GO	Good thermal stability and reliability, and Good thermal conductivity	[14]
n-nonadecane	P(St-co-MMA) <sup>d</sup>	Good chemical and thermal stability	[15]
n-octadecane	MF <sup>e</sup>	Good light-thermal conversion: high photothermal storage efficiency of 75%	[16]
Capric acid	PMMA <sup>f</sup>	Excellent insulation, and thermal stability	[17]

<sup>a</sup> PAMA: poly(allyl methacrylate).

<sup>b</sup> GO-CNT: Graphene oxide-carbon nanotubes.

<sup>c</sup> UF: urea-formaldehyde.

<sup>d</sup> P(St-co-MMA): poly(styrene-com-methyl methacrylate).

<sup>e</sup> MF: melanine-formaldehyde.

<sup>f</sup> PMMA: poly methyl methacrylate.

obtained the microcapsules using 750 and 1500 rpm. And finally, the ageing time was set to 4 and 8 h. Table 2 shows the samples prepared and the nomenclature used.

### 2.3. Characterization of the microcapsules

The structural, morphological, and thermal properties of the microcapsules were analysed using several instrumental techniques. X-ray diffraction (XRD) and Fourier transform infrared (FTIR) spectroscopy were used to analyse their structural properties. The XRD patterns were recorded using a D8 Advanced diffractometer supplied by Bruker with Cu-K $\alpha$  radiation. The scan conditions were from 10 to 70° in 2 $\theta$  with a resolution of 0.02°, 40 kV and 40 mA. The FTIR spectra were recorded using a T37+ HYP200 spectrophotometer supplied by Bruker. The range measured was between 400 and 4000 cm<sup>-1</sup> with a scan resolution of 1 cm<sup>-1</sup>. In addition, the morphology of the microcapsules was analysed by scanning electron microscopy (SEM), using a Nova NanoSEM 450 microscope supplied by Thermo Fischer. UV-Vis spectroscopy, in diffuse reflectance mode, was used to characterize the optical properties of the microcapsules, due to the semiconductor properties of ZnO. The optical band gap of the samples can be estimated from the spectra registered. The optical absorption coefficient ( $\alpha/S$ ) can be determined using the Kubelka-Munk formalism from the diffuse reflectance spectra according to  $(\alpha/S) = F(R) = [(1 - R)^2]/2R$  [33], where  $R$  is the percentage of reflected light, and  $\alpha$  and  $S$  are the absorption and the scattering coefficients. The Tauc plot relates the optical band gap and the incident photon energy, and is given by  $[F(R)h\nu]^p = A(h\nu - E_g)$  [34,35], where  $h\nu$  is the incident photon energy,  $A$  is a constant depending on the transition probability and  $E_g$  is the optical band gap. The power index  $p$  is related to the optical absorption process, this being 1/2 or 2 for an indirect or a directly allowed transition, respectively [36]. In the case of ZnO, the transition is direct, thus  $p = 2$  [36].

To analyse the properties of the microcapsules related with their application as a phase change material, the differential scanning calorimetry (DSC) technique was used (Netzsch, DSC 214 Polyma). The samples prepared were analysed performing 30 heating/cooling cycles between 0 and 60 °C at a rate of 1 °C/min. The melting point of C18 is 26-29 °C, so this range is appropriate to analyse the thermal properties of the microcapsules. Performing 30 heating/cooling cycles, the stability of the microcapsules can be analysed, but several other properties can also be obtained from these measurements, such as melting ( $\Delta H_m$ ) and crystallization ( $\Delta H_c$ ) enthalpies and melting ( $T_m$ ) and crystallization ( $T_c$ ) temperatures, from endothermic and exothermic plots. From the enthalpy values, the encapsulation efficiency ( $E_{en}$ ) and the energy storage efficiency ( $E_{es}$ ) can be estimated as

$$E_{en}(\%) = \frac{\Delta H_{m,mc}}{\Delta H_{m,C18}} \cdot 100 \quad (3)$$

$$E_{es}(\%) = \frac{\Delta H_{m,mc} - \Delta H_{c,mc}}{\Delta H_{m,C18} - \Delta H_{c,C18}} \cdot 100 \quad (4)$$

where the subscripts *mc* and *C18* refer to the microcapsules and the n-octadecane, respectively. Finally, from the encapsulation efficiency and

**Table 2**

Conditions of the synthesis of the C18@ZnO microcapsules.

Sample	C18:ZnSO <sub>4</sub>	Stirring rate/rpm	Ageing time/h
C18@ZnO_50/50_750_4	50:50	750	4
C18@ZnO_50/50_750_8		750	8
C18@ZnO_50/50_1500_4		1500	4
C18@ZnO_50/50_1500_8		1500	8
C18@ZnO_60/40_750_4	60:40	750	4
C18@ZnO_60/40_750_8		750	8
C18@ZnO_60/40_1500_4		1500	4
C18@ZnO_60/40_1500_8		1500	8

the energy storage efficiency, the thermal storage capacity can be calculated as

$$C_{es}(\%) = \frac{E_{es}}{E_{en}} \cdot 100 \quad (5)$$

Furthermore, isobaric specific heat was measured by means of temperature modulated differential scanning calorimetry (TMDSC) using a Netzsch, DSC 214 Polyma, setting a temperature program that involves: (i) a 5 °C/min ramp up to 60 °C and isothermal equilibration for 10 min to remove contaminants; (ii) a 1 °C/min ramp down to -5 °C; (iii) a 1 °C/min ramp from -5 °C to 22 °C under temperature-modulated conditions; (iv) a 1 °C/min ramp up to 35 °C; (v) a 1 °C/min ramp from 35 °C to 50 °C again under temperature-modulated conditions; and finally (vi) cooling at 1 °C/min. The temperature modulation was performed with oscillation amplitudes of  $\pm 1$  °C and a 120 s period.

Finally, as ZnO is a semiconductor with applications in photocatalysis, the performance as photocatalyst of the microcapsules synthesized was tested. To this end, the photodegradation of the crystal violet (CV) dye was analysed in the presence of the microcapsules using two irradiation sources: an actinic lamp emitting at 360 nm and a sun simulator (Abet Technologies, model Sun 3000). The initial concentration of the CV solution was 2·10<sup>-4</sup> M and the concentration of the photocatalyst, that is the microcapsules, was 0.6 g L<sup>-1</sup>. The photocatalyst/CV mixture was kept in darkness for 30 min and the reaction time was 5 h and 24 h for the actinic lamp and the sun simulator, respectively. The time in darkness before the photocatalysis process was established from the adsorption equilibrium tests in darkness, as is shown in the Supplementary Material (Fig. S1). The photodegradation of the CV dye was analysed by absorbance measurements. The absorbance was measured using a spectrometer (Ocean Optics, USB4000+) with a UV-vis-NIR light source (Ocean Optics, DH-2000-BAL).

### 3. Results and discussion

The microcapsules were characterized using several instrumental techniques to determine their structural, morphological, optical and thermal properties. Next, the results obtained for each technique are described.

#### 3.1. X-ray diffraction

Fig. 1 shows the XRD patterns obtained from the microcapsule samples described in Table 1. Three intense peaks are observed in all the patterns at 31.8°, 34.4° and 36.3°, which are assigned to the reflection of the (110), (002) and (101) planes. The relative intensity between these peaks in each pattern is not the same, probably because many ZnO crystals were formed with random orientation. In addition, five other less intense peaks are observed, and assigned in Fig. 1. These peaks are characteristic of ZnO with a hexagonal wurtzite structure and P63mc space group (JCPDS 36-1451). Therefore, XRD confirms the synthesis of ZnO.

From the reflection of the (101) planes, the crystal size was estimated using Scherrer's equation

$$t = \frac{K\lambda}{B \cos \theta} \quad (6)$$

where  $t$  is the crystal size;  $K$  is a constant with a value in this case of 0.85;  $\lambda$  is the wavelength of the x-ray (CuK $\alpha_1 = 1.5418$  Å),  $B$  is the full width at half maximum, and  $\theta$  is the Bragg angle [37]. The eight samples prepared, shown in Table 3, all obtained values in the 20–25 nm range, suggesting that the synthesis parameters do not have a significant impact on the crystallite size.

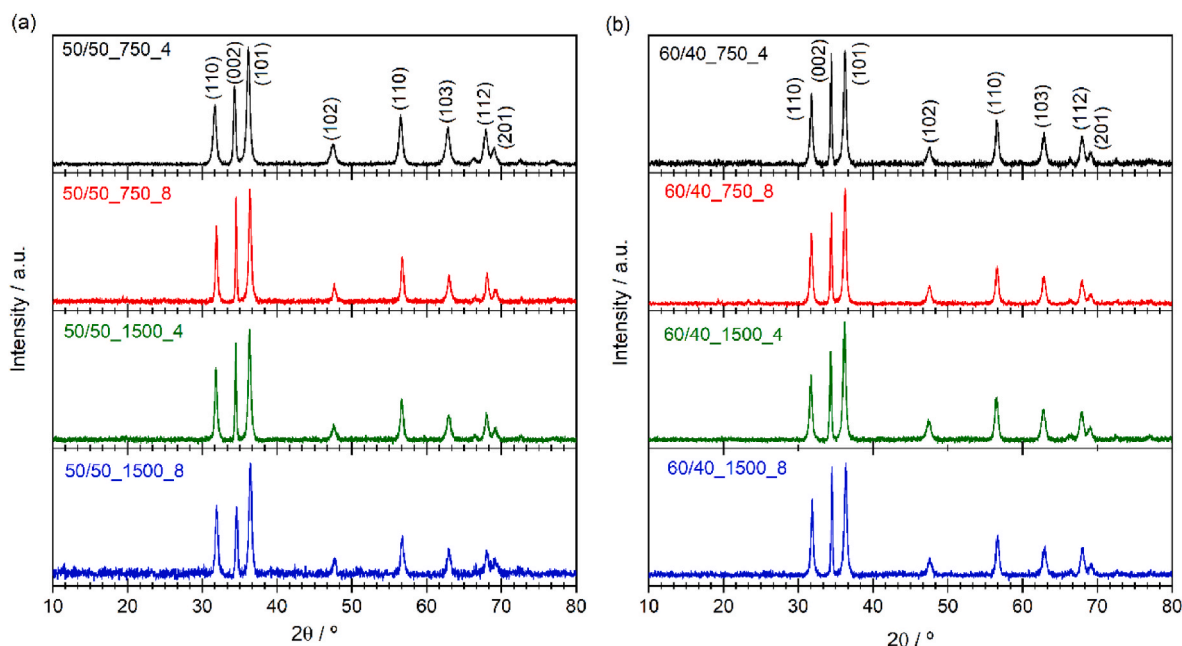


Fig. 1. XRD patterns for the microcapsules synthesized using a C18:ZnSO<sub>4</sub> of 50:50 (a) and 60:40 (b).

Table 3

Crystallite size of ZnO synthesized.

Sample	t/nm	Sample	t/nm
C18@ZnO_50/50_750_4	20	C18@ZnO_60/40_750_4	25
C18@ZnO_50/50_750_8	23	C18@ZnO_60/40_750_8	25
C18@ZnO_50/50_1500_4	24	C18@ZnO_60/40_1500_4	25
C18@ZnO_50/50_1500_8	23	C18@ZnO_60/40_1500_8	23

### 3.2. FTIR spectroscopy

Fig. 2 shows the FTIR spectra obtained for pure C18, pure ZnO, and all the C18@ZnO microcapsules prepared. Fig. 2a shows the spectrum for C18. The stretching band for C–H bonds of methyl groups, –CH<sub>3</sub> and –CH<sub>2</sub>–, is observed at about 2800–3000 cm<sup>-1</sup>; and the stretching band for C–C bonds is also observed at 1600 cm<sup>-1</sup>. Several bending bands of C–H bonds are observed at about 1400, 1300 and 750 cm<sup>-1</sup>. Fig. 2b shows the spectrum for pure ZnO. An intense bending band is observed at about 500 cm<sup>-1</sup> while the typical stretching band for O–H bonds is observed at about 3500 cm<sup>-1</sup>. Both spectra shown in Fig. 2a and b are typical for pure C18 and ZnO. All these typical bands for both compounds are observed in the spectra obtained for the C18@ZnO microcapsules, shown in Fig. 2c and d, confirming the presence of both compounds in the microcapsules prepared. The spectra of the microcapsules show the typical bands for both compounds, C18 and ZnO, with no significant impact on the respective bands. A decrease of the intensity of the C18 bands may be observed, but they can be clearly assigned to C18. Therefore, these FTIR spectra are evidence of the encapsulation of C18 using ZnO.

#### 3.2.1. Scanning electron microscopy

Fig. 3 shows SEM images of the microcapsules synthesized using a 50:50 ratio (C18:ZnSO<sub>4</sub>). A morphology close to spherical is observed, and small nanoparticles were found on their surface. The appearance, morphology and size of these particles are similar to data previously reported for pure ZnO [38,39]. Furthermore, it seems that these small particles are forming the ZnO capsules, as is possible to observe in the images, which is also coherent with the crystallite sizes obtained from XRD. When the 60:40 ratio is used, these small nanoparticles are not observed, probably due to there being less Zn in the synthesis. What is

more, in this case, different structures are observed (see images of C18@ZnO\_60/40\_1500\_4 and C18@ZnO\_60/40\_1500\_8 in Fig. 4). In both cases, it seems that these microcapsules have not been completely formed, probably due to the smaller amount of Zn. In both samples, fully formed capsules were also observed that measure about 10 μm in all cases. The microcapsules were subjected to a grinding treatment to observe their internal structure. The broken capsule in Fig. 5 shows a *honeycomb* microstructure with numerous individual cells in which the C18 is housed. In addition, Fig. 4 below shows a particle with the *honeycomb* structure, which is also observed in Fig. 5. Thus, it is possible that this structure is covered by ZnO to form the microcapsules, but the particle shown at the bottom right of Fig. 4 was not completely formed. Finally, Fig. S2 in Supplementary Material shows a low magnification SEM image of the C18@ZnO\_50/50\_750\_4 sample in which the homogeneity of the sample is observed, this being representative of all the samples.

#### 3.3. DR-UV-vis spectroscopy

The optical properties of the microcapsules synthesized were studied using UV–Vis spectroscopy in diffuse reflectance mode. Fig. 6 shows the spectra recorded for all the microcapsules, in terms of the Kubelka-Munk function. The spectra obtained show an absorption band below 400 nm, as expected. From these spectra, and by using the Tauc plot, which was described above, the band gap energy values were estimated, and are shown in Table 4. We can observe that the values do not change significantly, ranging between 3 and 3.2 eV. These values are coherent with the typical values reported in the literature for ZnO nanoparticles [40,41]. Therefore, the impact of the C18 on the optical band gap values of ZnO is negligible.

#### 3.4. Thermal analysis

The microcapsules prepared are intended for use in energy storage, so their thermal characterization is of great interest. It is essential to know the enthalpy of the phase change and their thermal stability. Melting and crystallization enthalpies, ΔH<sub>m</sub> and ΔH<sub>c</sub>, and temperatures, T<sub>m</sub> and T<sub>c</sub>, were estimated by DSC cycles for all the microcapsules and for pure C18. From these values, the encapsulation efficiency (E<sub>en</sub>), the energy storage efficiency (E<sub>es</sub>) and the energy storage capacity (C<sub>es</sub>) were

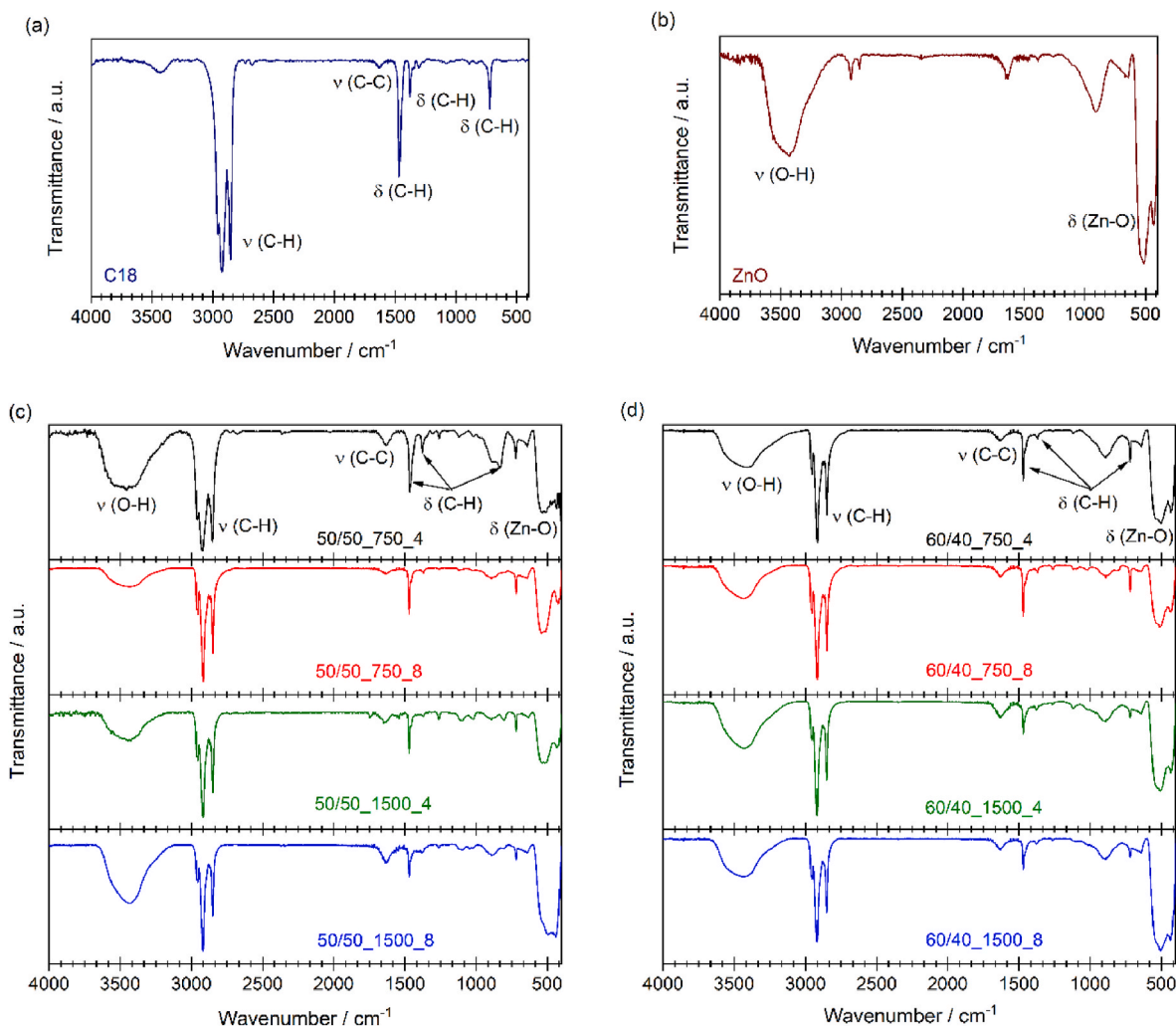


Fig. 2. FTIR spectra of (a) pure C18; (b) pure ZnO; (c) C18@ZnO microcapsules with a 50:50 ratio (C18:ZnSO<sub>4</sub>); and (d) microcapsules with a 60:40 ratio (C18:ZnSO<sub>4</sub>).

calculated according to Equations (3)–(5). The results obtained are shown in Table 5. Typically, the enthalpy value for the microcapsules was lower than that of C18 because of the presence of ZnO, which presents a lower latent heat. That is, the microcapsules contain less C18, the component with a higher enthalpy per unit of mass, due to the presence of ZnO. This can be explained by the smaller amount of PCM in the capsule samples with regard to the pure C18 because the mass of the samples used in the DSC measurements is similar, and the capsules include a portion of ZnO. Moreover, the phase change temperature values for the microcapsules are close to that obtained for pure C18. Therefore, the microcapsules can be used in applications in which a phase change of around 25 °C is needed. The presence of ZnO as the outer material of the capsule does not affect significantly the phase change temperature in either the melting or crystallization processes in the microcapsules. According to the encapsulation and energy storage efficiency values, calculated according to Eqs. (3) and (4) (see Experimental section), the three samples that presented the best values for encapsulation efficiency and energy storage capacity were selected, namely C18@ZnO\_50/50\_750\_4, C18@ZnO\_50/50\_750\_8 and C18@ZnO\_60/40\_750\_4. These three samples showed an energy storage capacity of 100%, which means that all the C18 inside the microcapsules is able to store thermal energy and release latent heat. They show an encapsulation efficiency of 21.3%, 19.4% and 23.1%, respectively. These values are lower than those found in studies in the literature, many of which lack details of how the microcapsules were cleaned, and

the presence of PCM on the outside of the microcapsule can falsify some results. Our experience leads us to believe that cleaning is a more complicated process than expected. According to the synthesis procedure, a stirring rate of 750 rpm is seen to favour the encapsulation of C18 because the samples prepared in this way show the highest encapsulation efficiency ( $E_{en}$ ) and thermal storage capacity ( $C_{es}$ ), as shown in Table 5. This probably occurs because a higher stirring rate would lead to a decrease in the diameter of the drops in the emulsion formed when water and C18 are mixed, and therefore the amount of PCM encapsulated is very low with regard to amount of oxide [42]. In addition, a core@shell ratio of 60:40 and a stirring rate of 750 rpm (C18@ZnO\_60/40\_750\_4) improved the encapsulation and thermal behaviour, probably because more C18 can be encapsulated. No correlation was observed between the ageing time and the thermal behaviour.

The three samples selected were subjected to 30 cycles of melting and crystallization following the DSC technique. All of the DSC plots obtained are shown in Fig. S3 in the Supplementary Material. There are similarities between the profiles of the DSC plots of the pure PCM and its corresponding microcapsule. The microcapsule samples are powder, so the presence of the phase change peaks in the plots is evidence of the formation of the capsules including the PCMs inside. These thermograms show that the microcapsules present high stability. A small peak can also be seen in the C18@ZnO\_50/50\_750\_8 sample at 26.4 °C. This peak can be assigned to the formation of a transition phase, probably due to a rotator phase. This rotator phase is a metastable phase which typically

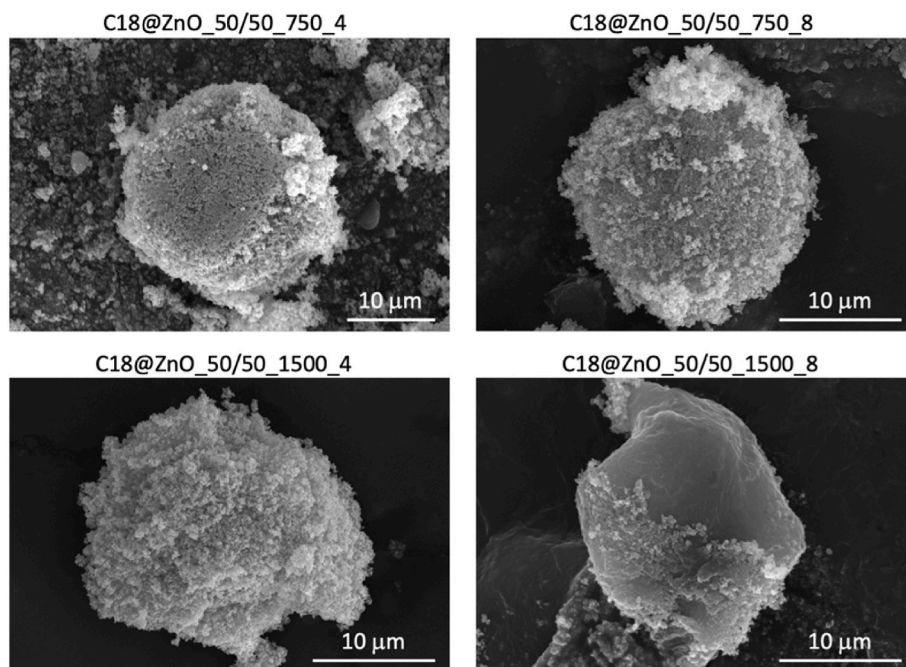


Fig. 3. SEM images for C18@ZnO microcapsules prepared using a 50:50 ratio (C18:ZnSO<sub>4</sub>).

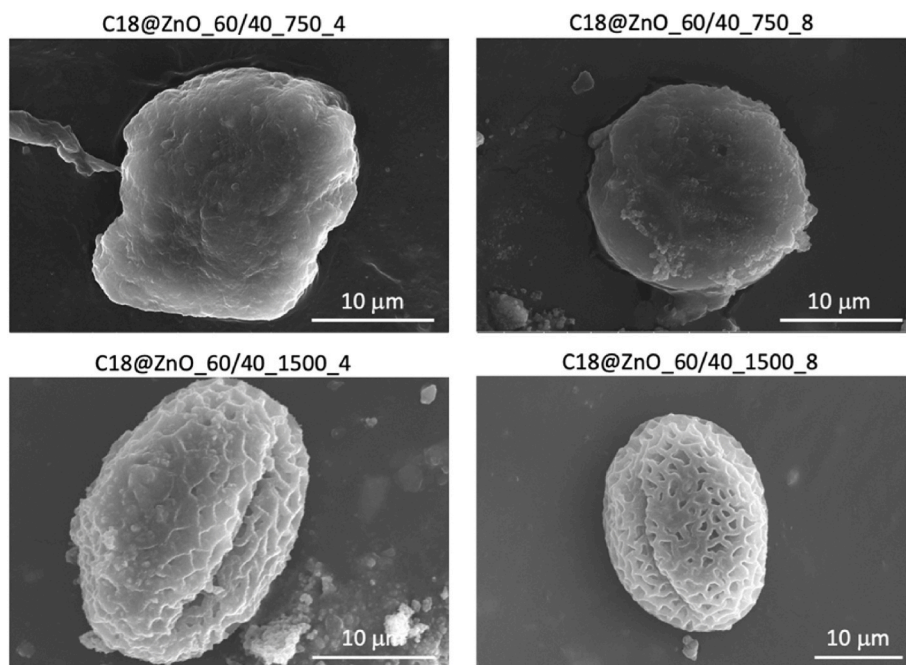


Fig. 4. SEM images for C18@ZnO microcapsules prepared using a 60:40 ratio (C18:ZnSO<sub>4</sub>).

appears at temperatures higher than the crystallization process [43,44]. In addition, from these cycles, the values of the melting and crystallization enthalpies were estimated for the three selected microcapsules and for the pure C18 to analyse the stability of the microcapsules. Fig. 7 shows the values obtained. The melting enthalpy for pure C18 was found to be about  $230 \text{ J g}^{-1}$ , which is coherent with values reported in the literature [45]. A slight decrease of about  $3 \text{ J g}^{-1}$  of was found for this value after 30 cycles, as Fig. 7d shows. The values for the microcapsules remain stable, as is observed in Fig. 7a–c. Therefore, the ZnO-based microcapsules are able to protect the PCM and keep it inside.

### 3.5. Isobaric specific heat

The isobaric specific heat of the microcapsules, the pure C18 and the ZnO was measured by using temperature modulated differential scanning calorimetry in the range between  $-5$  and  $55 \text{ }^\circ\text{C}$ . Fig. 8 shows the values obtained. Those between  $20$  and  $32 \text{ }^\circ\text{C}$  are missing because of the phase change of C18. The evolution of the isobaric specific heat with temperature is quasi linear in all cases, except in the range between  $15$  and  $20 \text{ }^\circ\text{C}$  for the microcapsules and pure C18 because the solid to liquid phase change of C18 is beginning. However, the most interesting result is that two microcapsules synthesized (C18@ZnO\_50/50\_750\_4 and

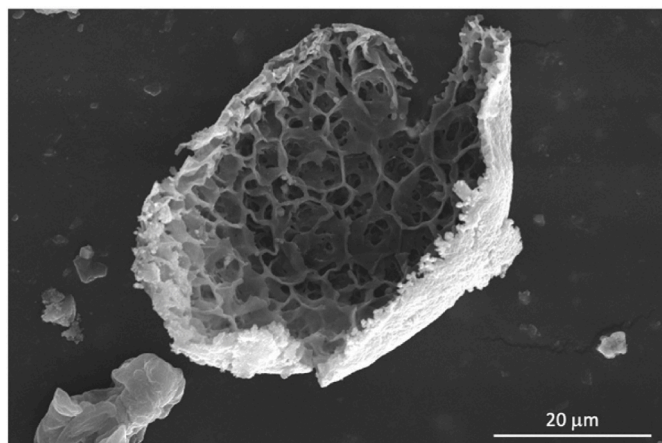


Fig. 5. A broken microcapsule of C18@ZnO\_60/40\_750\_8 sample observed by SEM.

C18@ZnO\_60/40\_750\_4) show values higher than that of the pure ZnO. This is interesting because ZnO has several building-related applications of interest, and replacing pure ZnO with ZnO-based microcapsules opens the option of storing energy and releasing energy from the latent heat of the PCM. In this sense, the C18@ZnO\_60/40\_750\_4 sample showed high isobaric specific heat values and the best encapsulation and energy storage efficiencies, according to the results shown in Table 5. Therefore, this sample may be promising for this kind of applications.

### 3.6. Photocatalytic activity

The performance of the microcapsules as a photocatalyst was analysed by using photodegradation tests of CV dye. Photolysis tests were performed using both the irradiation sources used in the photocatalytic tests, namely an actinic lamp and a sun simulator. The mixture of CV dye and the microcapsules was kept at a temperature of 18 °C so that the C18 inside the microcapsules remained in solid phase to avoid the effect of the energy storage of the C18. Furthermore, the pH was kept at 8 in all the tests. The evolution of the photolysis and photodegradation tests was performed by UV-vis measurements. From absorbance values, the CV concentration at each time was calculated using the Lambert-Beer law, which relates the absorbance ( $A$ ) with concentration ( $C$ ) as  $A = \epsilon Cl$ , where  $l$  is the optical path (1 cm), and  $\epsilon$  the molar absorption coefficient, which is 77770 L mol<sup>-1</sup> cm<sup>-1</sup> for CV dye [46]. Fig. 9 shows the results obtained from these tests given as the ratio of the concentration at each time and the initial concentration ( $C/C_0$ ) versus time. After 5 h, the

degradation of CV dye was higher when a sun simulator was used as the irradiation source. We can also observe that the photolysis using the UV irradiation (actinic lamp) leads to less degradation than in the photocatalytic tests performed using the same actinic lamp, as is shown in Fig. 9a. This means the microcapsules show photocatalytic activity. On the other hand, using a sun simulator (see Fig. 9b), the photolysis is higher than in the case of the actinic lamp. Moreover, using a sun simulator, the presence of microcapsules increases the rate of degradation, meaning that the microcapsules show photocatalytic activity under visible light too. Furthermore, in accordance with the results obtained (Fig. 9), the photodegradation of CV dye follows pseudo-first-order

Table 4  
Band gap energy values for all the microcapsules synthesized.

Sample	$E_g$ /eV	Sample	$E_g$ /eV
C18@ZnO_50/50_750_4	3.17 ± 0.03	C18@ZnO_60/40_750_4	3.00 ± 0.03
C18@ZnO_50/50_750_8	3.04 ± 0.02	C18@ZnO_60/40_750_8	3.21 ± 0.03
C18@ZnO_50/50_1500_4	3.14 ± 0.01	C18@ZnO_60/40_1500_4	3.17 ± 0.03
C18@ZnO_50/50_1500_8	3.20 ± 0.03	C18@ZnO_60/40_1500_8	3.14 ± 0.01

Table 5  
Melting and crystallization enthalpy values,  $\Delta H_m$  and  $\Delta H_c$ , and temperatures,  $T_m$  and  $T_c$ , and the encapsulation efficiency ( $E_{en}$ ), energy storage efficiency ( $E_{es}$ ) and energy storage capacity ( $C_{es}$ ).

Samples	$\Delta H_m$ /J g <sup>-1</sup>	$-\Delta H_c$ /J g <sup>-1</sup>	$T_m$ /°C	$T_c$ /°C	$E_{en}$ /%	$E_{es}$ /%	$C_{es}$ /%
C18	230.9	231.0	25.9	24.5	–	–	–
C18@ZnO_50/50_750_4	49.2	49.0	24.1	24.1	21.3	21.3	100
C18@ZnO_50/50_750_8	44.8	44.7	24.9	24.6	19.4	19.4	100
C18@ZnO_50/50_1500_4	31.8	31.2	23.6	23.3	13.8	13.6	98
C18@ZnO_50/50_1500_8	27.9	26.2	21.7	22.1	12.1	11.7	96
C18@ZnO_60/40_750_4	53.3	53.2	25.0	24.5	23.1	23.1	100
C18@ZnO_60/40_750_8	31.5	30.7	23.9	23.2	13.6	13.4	98
C18@ZnO_60/40_1500_4	25.5	24.7	23.2	22.6	11.0	10.8	98
C18@ZnO_60/40_1500_8	29.1	28.2	23.5	23.0	12.6	12.4	98

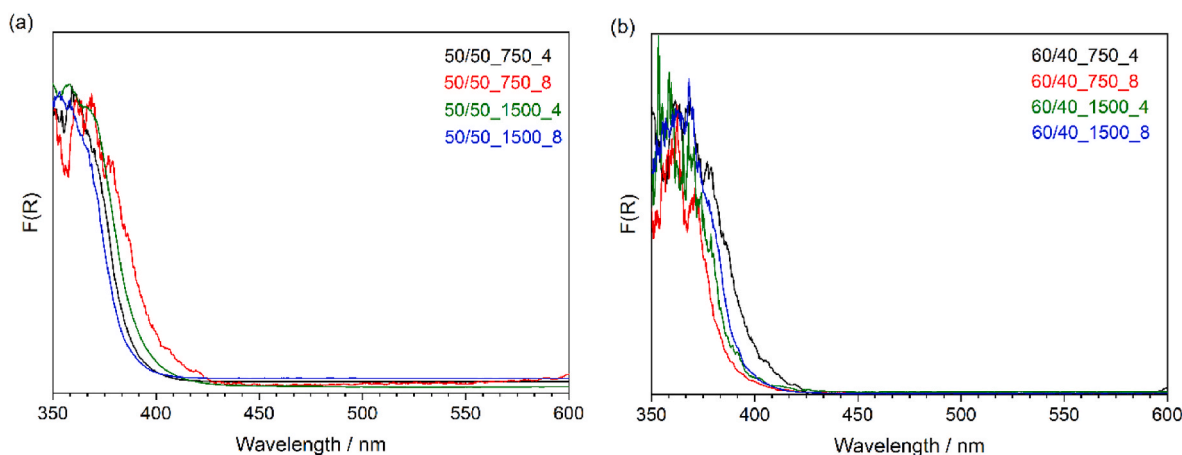


Fig. 6. UV-Vis spectra in diffuse reflectance mode for (a) C18@ZnO microcapsules with a 50:50 ratio (C18:ZnSO<sub>4</sub>); and (b) microcapsules with a 60:40 ratio (C18:ZnSO<sub>4</sub>).

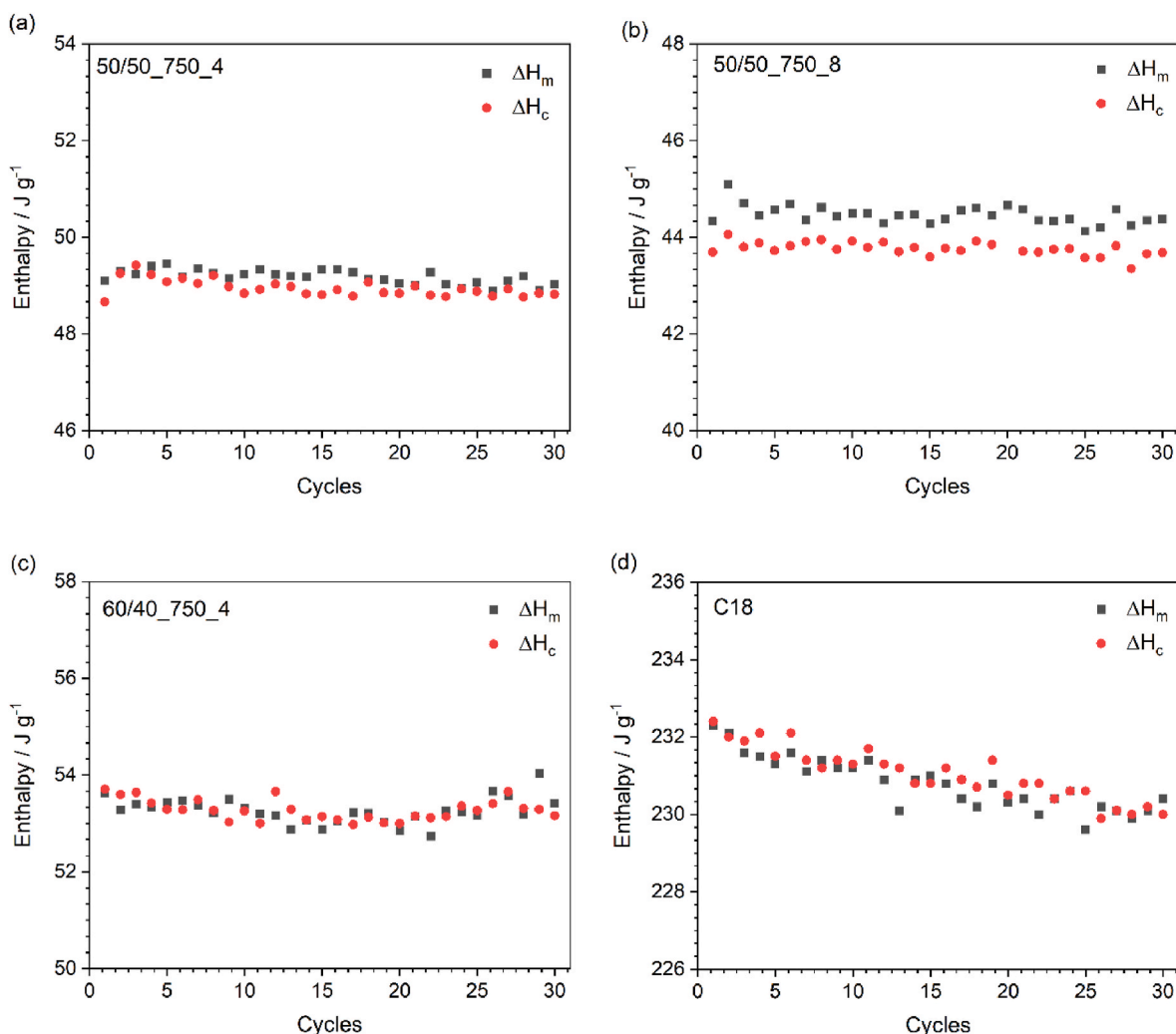


Fig. 7. Melting and crystallization enthalpies for the three microcapsules selected (a–c) and for pure C18 (d).

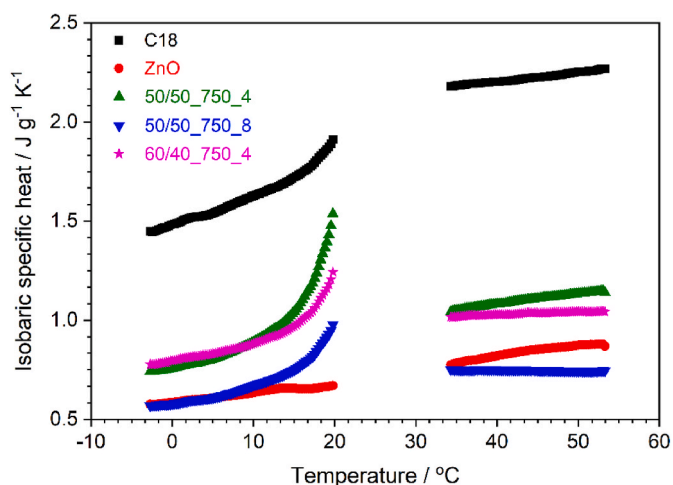


Fig. 8. Isobaric specific heat values for pure C18 and ZnO, and the three microcapsules selected.

kinetics, which can be described as  $\ln(C_0/C) = -kKt = k_{app}t$ , where  $C_0$  is the initial concentration of CV dye,  $C$  is the concentration of the CV dye with irradiation time  $t$ ,  $k$  is the reaction constant,  $K$  is the adsorption constant, and  $k_{app}$  is the apparent rate constant [47]. Table 6 shows the

values of the apparent rate constant obtained. Using the actinic lamp, under UV irradiation, the rate for the photocatalytic tests is higher than the photolysis test, which means the microcapsules show photocatalytic activity, the C18@ZnO<sub>60/40\_750\_4</sub> capsules showing the best results. From these results, we can propose a mechanism for the photocatalytic process using UV irradiation. This probably begins with the excitation of an electron from the valence band to the conduction band of ZnO thanks to the UV irradiation, followed by a reaction with water or dissolved oxygen to produce super oxidizing agents such as OH<sup>•</sup>, which can degrade the CV dye.

In addition, under visible light from a sun simulator, the photolysis is higher and the degradation of CV shows a high thermal contribution. The presence of microcapsules results in a higher degradation rate, the C18@ZnO<sub>60/40\_750\_4</sub> sample again showing the best photocatalytic activity. In this case, we can propose a mechanism from the results obtained. The proposed mechanism of the photocatalysis process is not produced by the excitation of an electron towards the conduction band, because the irradiation is not energetic enough. It is probably a dye-sensitized mechanism in which the photons are absorbed by CV molecules adsorbed onto the ZnO surface, after which the excited electrons are transferred to the conduction band, following the process described above. According to the results obtained, this mechanism seems to be more efficient.

The ZnO-based microcapsules synthesized presented photocatalytic activity which provides the option of using them to remove pollutants from buildings. The semiconductor properties of ZnO have been

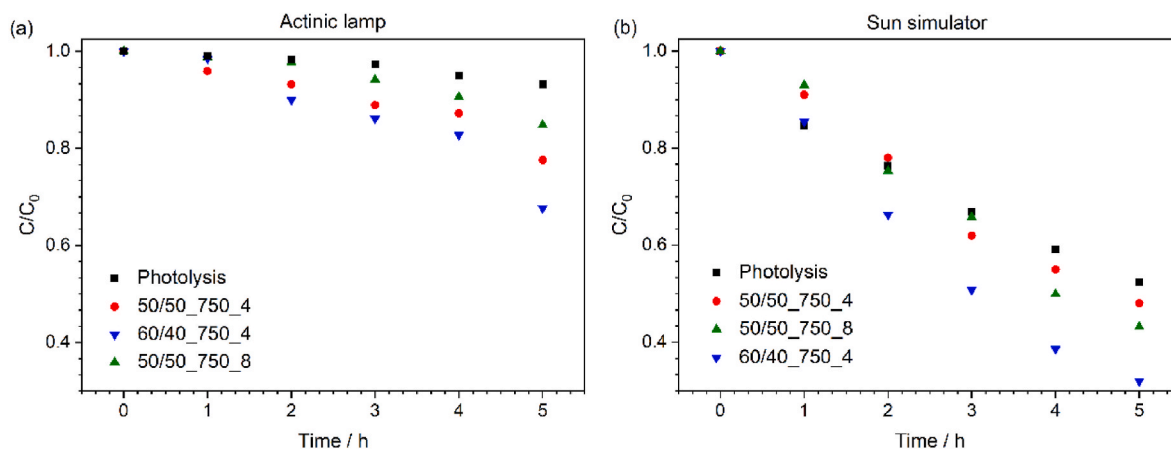


Fig. 9. Photolysis and photocatalytic tests using an actinic lamp (a) and a sun simulator (b).

Table 6

Values of the apparent rate constant for the photolysis and photocatalytic tests performed.

Test/photocatalyst	$k_{app}/h^{-1}$	
	Actinic lamp	Sun simulator
Photolysis	0.0139	0.1266
C18@ZnO_50/50_750_4	0.0458	0.1546
C18@ZnO_50/50_750_8	0.0319	0.1772
C18@ZnO_60/40_750_4	0.0720	0.2384

reported and, for example, its application showing antifungal activity embedded in cements with applications in buildings has been studied [48,49], as well as its photocatalytic activity to remove contaminants in construction materials [50].

#### 4. Conclusions

Microcapsules based on ZnO and n-octadecane were synthesized and characterized to determine their physical and chemical properties. The main results found in this work are.

- The comprehensive characterization performed confirmed the formation of ZnO microcapsules containing C18. A quasi-spherical morphology was observed by means of SEM. The internal part of the microcapsules presented a honeycomb structure.
- The highest encapsulation efficiency value found was 23.1% for the samples with a 60:40 ratio (C18:ZnSO<sub>4</sub>), a stirring rate of 750 rpm and ageing time of 4 h.
- Heating/cooling cycles were also performed, and the microcapsules were found to present good stability. Thus, ZnO-based microcapsules are able to protect the PCM and keep it inside.
- We observed an increase in the isobaric specific heat of some microcapsules with respect to the ZnO. This is interesting because ZnO has several building-related applications and the change from pure ZnO to ZnO-based microcapsules provides the option of storing released energy from the latent heat of the PCM.
- Finally, the photocatalytic activity of the microcapsules was confirmed under UV and visible irradiation, which is of interest because the microcapsules can be used for removing organic pollutants from buildings.

Therefore, the microcapsules synthesized based on ZnO showed properties that make the of interest for a wide range of applications, such as those involving thermal energy storage and photocatalysis.

#### CRedit authorship contribution statement

**Javier Sánchez-Fernández:** Methodology, Investigation, Writing – original draft. **Teresa Aguilar:** Conceptualization, Investigation, Formal analysis. **Ivan Carrillo-Berdugo:** Investigation, Methodology. **Juan Jesús Gallardo:** Investigation, Methodology. **Javier Navas:** Writing – review & editing, Supervision, Project administration, Funding acquisition.

#### Declaration of competing interest

The authors declare that they have no known competing financial interests or personal relationships that could have appeared to influence the work reported in this paper.

#### Data availability

The authors do not have permission to share data.

#### Acknowledgments

I.C.-B. thanks *Ministerio de Universidades del Gobierno de España* for endorsing his postdoctoral position at the University of Cadiz with a *Margarita Salas* fellowship, granted within the call for *Recualificación del Sistema Universitario Español para 2021–2023*, funded by the NextGeneration EU programme of the European Union. The group acknowledges *Ministerio de Ciencia e Innovación del Gobierno de España* [grants number RTI2018-096393-B-I00, UNCA15-CE-2945]. This research was also funded by the Andalucía ERDF Operational Programme 2014–2020, managed by *Consejería de Transformación Económica, Industria, Conocimiento y Universidades de la Junta de Andalucía* [grant FEDER-UCA18-107510].

#### Appendix A. Supplementary data

Supplementary data to this article can be found online at <https://doi.org/10.1016/j.matchemphys.2023.127501>.

#### References

- [1] E. Erdem, Why P2X must be the part of the energy solution? *Environ. Prog. Sustain.* 40 (3) (2021) <https://doi.org/10.1002/ep.13545>.
- [2] W. Aftab, H.Y. Huang, W.H. Wu, Z.B. Liang, A. Mahmood, R.Q. Zou, Nanoconfined phase change materials for thermal energy applications, *Energy Environ. Sci.* 11 (2018) 1392–1424, <https://doi.org/10.1039/c7ee03587j>.
- [3] M. Li, Z.S. Wu, J.M. Tan, Properties of form-stable paraffin/silicon dioxide/expanded graphite phase change composites prepared by sol-gel method, *Appl. Energy* 92 (2012) 456–461, <https://doi.org/10.1016/j.apenergy.2011.11.018>.

- [4] F. Agyenim, N. Hewitt, P. Eames, M. Smyth, A review of materials, heat transfer and phase change problem formulation for latent heat thermal energy storage systems (LHTESS), *Renew. Sustain. Energy Rev.* 14 (2010) 615–628, <https://doi.org/10.1016/j.rser.2009.10.015>.
- [5] W.G. Su, J. Darkwa, G. Kokogiannakis, Review of solid-liquid phase change materials and their encapsulation technologies, *Renew. Sustain. Energy Rev.* 48 (2015) 373–391, <https://doi.org/10.1016/j.rser.2015.04.044>.
- [6] M. Hunger, A.G. Entrop, I. Mandilaras, H.J.H. Brouwers, M. Founti, The behavior of self-compacting concrete containing micro-encapsulated Phase Change Materials, *Cement Concr. Compos.* 31 (2009) 731–743, <https://doi.org/10.1016/j.cemconcomp.2009.08.002>.
- [7] G.V. Belessiotis, K.G. Papadokostaki, E.P. Favvas, E.K. Efthimiadou, S. Karellas, Preparation and investigation of distinct and shape stable paraffin/SiO<sub>2</sub> composite PCM nanospheres, *Energy Convers. Manag.* 168 (2018) 382–394, <https://doi.org/10.1016/j.enconman.2018.04.059>.
- [8] Y. Konuklu, H. Burak Akar, Promising palmitic acid/poly(allyl methacrylate) microcapsules for thermal management applications, *Energy* 262 (2023), 125491, <https://doi.org/10.1016/j.energy.2022.125491>.
- [9] F. He, X. Wang, D. Wu, New approach for sol-gel synthesis of microencapsulated n-octadecane phase change material with silica wall using sodium silicate precursor, *Energy* 67 (2014) 2118–2132, <https://doi.org/10.1016/j.energy.2013.11.088>.
- [10] Z. Wang, Y. Chen, Synthesis and characteristics of microencapsulated myristic acid with TiO<sub>2</sub> as composite thermal energy storage materials, *Mater. Sci.* 27 (2021) 451–457, <https://doi.org/10.5755/j02.ms.25098>.
- [11] Q. Li, X. Ma, X. Zhang, J. Ma, J. Liu, X. Hu, Y. Lan, Preparation and properties of Al/Al<sub>2</sub>O<sub>3</sub> core-shell microencapsulated phase change material, *J. Alloys Compd.* 888 (2021), 161606, <https://doi.org/10.1016/j.jallcom.2021.161606>.
- [12] D.S. Ezhumalai, G. Sriharan, S. Harikrishnan, Improved thermal energy storage behavior of CuO/palmitic acid composite as phase change material, *Mater. Today Proc.* 5 (2018) 14618–14627, <https://doi.org/10.1016/j.matpr.2018.03.053>.
- [13] Z.L. Zheng, J.D. Jin, G.K. Xu, J.L. Zou, U. Wais, A. Beckett, Highly stable and conductive microcapsules for enhancement of joule heating performance, *ACS Nano* 11 (2016) 4695–4703, <https://doi.org/10.1021/acsnano.6b01104>.
- [14] Z. Qiao, J. Mao, Enhanced thermal properties with graphene oxide in the urea-formaldehyde microcapsules containing paraffin PCMs, *J. Microencapsul.* 34 (1) (2017) 1–9, <https://doi.org/10.1080/02652048.2016.1267811>.
- [15] T. Khadiran, M.Z. Hussein, Z. Zainal, R. Rusli, Nano-encapsulated n-nonadecane using vinyl copolymer shell for thermal energy storage medium, *Macromol. Res.* 23 (7) (2015) 658–669, <https://doi.org/10.1007/s13233-015-3088-z>.
- [16] C.W. Huang, Q.T. Li, Y.B. Yang, S. Wei, R. Ji, Q.F. Zhang, Y.C. Zhu, H.Z. Zhang, F. Xu, L.X. Sun, Y.P. Xia, A novel bifunctional microencapsulated phase change material loaded with ZnO for thermal energy storage and light-thermal energy conversion, *Sustain. Energy Fuels* 4 (10) (2020) 5203–5214, <https://doi.org/10.1039/D0SE000718H>.
- [17] C.C. Chang, Y.L. Tsai, J.J. Chiu, H. Chen, Preparation of phase change materials microcapsules by using PMMA network-silica hybrid shell via sol-gel process, *J. Appl. Polym. Sci.* 112 (3) (2009) 1850–1857, <https://doi.org/10.1002/app.29742>.
- [18] E.S. Nour, O. Nur, M. Willander, Zinc oxide piezoelectric nano-generators for low frequency applications, *Semicond. Sci. Technol.* 32 (2017), 064005, <https://doi.org/10.1088/1361-6641/aa6bde>.
- [19] E. Muchuwani, T.S. Sathiaraj, H. Nyakoty, Synthesis and characterization of zinc oxide thin films for optoelectronic applications, *Heliyon* 3 (2017), e00285, <https://doi.org/10.1016/j.heliyon.2017.e00285>.
- [20] J. Yang, X. Kong, W. Jiang, J. Cao, P. Zou, H. Luan, L. Yang, Size-controllable synthesis and photocatalytic performance of ZnO hollow spheres, *Mater. Sci. Semicond. Process.* 40 (2015) 713–719, <https://doi.org/10.1016/j.mssp.2015.07.071>.
- [21] M. Mansournia, S. Rafizadeh, S.M. Hosseinpour-Mashkani, Hydrothermal synthesis, characterization and light harvesting applications of zinc oxide nanostructures, *J. Mater. Sci. Mater. Electron.* 26 (8) (2015) 5839–5846, <https://doi.org/10.1007/s10854-015-3144-7>.
- [22] M. Mansournia, S. Rafizadeh, S.M. Hosseinpour-Mashkani, An ammonia vapor-based approach to ZnO nanostructures and their study as photocatalyst material, *Ceram. Int.* 42 (1) (2016) 907–916, <https://doi.org/10.1016/j.ceramint.2015.09.017>.
- [23] M.H. Aleinawi, A.U. Ammar, M. Buldu-Akturk, N.S. Turhan, S. Nadupalli, E. Erdem, Spectroscopic probing of Mn-doped ZnO nanowires synthesized via a microwave-assisted route, *J. Phys. Chem. C* 126 (8) (2022) 4229–4240, <https://doi.org/10.1021/acs.jpcc.2c00009>.
- [24] M. Buldu-Akturk, M. Toufani, A. Tufani, E. Erdem, ZnO and reduced graphene oxide electrodes for all-in-one supercapacitor devices, *Nanoscale* 14 (8) (2022) 3269–3278, <https://doi.org/10.1039/D2NR00018K>.
- [25] S. Nadupalli, S. Repp, S. Weber, E. Erdem, About defect phenomena in ZnO nanocrystals, *Nanoscale* 13 (20) (2021) 9160–9171, <https://doi.org/10.1039/D1NR00943E>.
- [26] S. Najib, F. Bakan, N. Abdullayeva, R. Bahariqushchi, S. Kasap, G. Franzo, M. Sankir, N.D. Sankir, S. Mirabella, E. Erdem, Tailoring morphology to control defect structures in ZnO electrodes for high-performance supercapacitor devices, *Nanoscale* 12 (30) (2020) 16162–16172, <https://doi.org/10.1039/D0NR03921G>.
- [27] M. Toufani, S. Kasap, A. Tufani, F. Bakan, S. Weber, E. Erdem, Synergy of nano-ZnO and 3D-graphene foam electrodes for asymmetric supercapacitor devices, *Nanoscale* 12 (24) (2020) 12790–12800, <https://doi.org/10.1039/D0NR02028A>.
- [28] M.N.H. Mia, M.F. Pervez, M.K. Hossain, M.R. Rahman, M.J. Uddin, M.A. Al Mashud, H.K. Ghosh, M. Hoq, Influence of Mg content on tailoring optical bandgap of Mg-doped ZnO thin film prepared by sol-gel method, *Results Phys.* 7 (2017) 2683–2691, <https://doi.org/10.1016/j.rinp.2017.07.047>.
- [29] M.F. Pervez, M.N.H. Mia, S. Hossain, S.M.K. Saha, M.H. Ali, P. Sarker, M. K. Hossain, M.A. Matin, M. Hoq, M.A.M. Chowdhury, Influence of total absorbed dose of gamma radiation on optical bandgap and structural properties of Mg-doped zinc oxide, *Optik* 162 (2018) 140–150, <https://doi.org/10.1016/j.jlpe.2018.02.063>.
- [30] M.N.H. Mia, U. Habiba, M.F. Pervez, H. Kabir, S. Nur, M.F. Hossen, S.K. Sen, M. K. Hossain, M.A. Iftekhhar, M.M. Rahman, Investigation of aluminum doping on structural and optical characteristics of sol-gel assisted spin-coated nano-structured zinc oxide thin films, *Appl Phys a-Mater* 126 (3) (2020), <https://doi.org/10.1007/s00339-020-3332-z>.
- [31] F. Li, X. Wang, D. Wu, Fabrication of multifunctional microcapsules containing n-eicosane core and zinc oxide shell for low-temperature energy storage, photocatalysis, and antibiosis, *Energy Convers. Manag.* 106 (2015) 873–875, <https://doi.org/10.1016/j.enconman.2015.10.026>.
- [32] W. Jia, S. Dang, H. Liu, Z. Zhang, C. Yu, X. Liu, B. Xu, Evidence of the formation mechanism of ZnO in aqueous solution, *Mater. Lett.* 82 (2012) 99–101, <https://doi.org/10.1016/j.matlet.2012.05.013>.
- [33] L.F. Gate, Comparison of photon diffusion-model and kubelka-munk equation with exact solution of radiative transport-equation, *Appl. Opt.* 13 (2) (1974) 236–238, <https://opg.optica.org/ao/abstract.cfm?URI=ao-13-2-236>.
- [34] J. Navas, A. Sanchez-Coronilla, T. Aguilar, N.C. Hernandez, D.M. de los Santos, J. Sanchez-Marquez, D. Zorrilla, C. Fernandez-Lorenzo, R. Alcantara, J. Martin-Calleja, Experimental and theoretical study of the electronic properties of Cu-doped anatase TiO<sub>2</sub>, *Phys. Chem. Chem. Phys.* 16 (8) (2014) 3835–3845, <https://doi.org/10.1039/c3cp54273d>.
- [35] N. Serpone, D. Lawless, R. Khairutdinov, Size effects on the photophysical properties of colloidal anatase TiO<sub>2</sub> particles - size quantization or direct transitions in this indirect semiconductor, *J. Phys. Chem. Us* 99 (45) (1995) 16646–16654, <https://doi.org/10.1021/j100045a026>.
- [36] J.B. Coulter, D.P. Birnie, Assessing Tauc plot slope quantification: ZnO thin films as a model system, *Phys. Status Solidi B* 255 (3) (2018), 1700393, <https://doi.org/10.1002/psb.201700393>.
- [37] S. Gurmen, B. Ebin, Production and characterization of the nanostructured hollow iron oxide spheres and nanoparticles by aerosol route, *J. Alloys Compd.* 492 (1–2) (2010) 585–589, <https://doi.org/10.1016/j.jallcom.2009.11.186>.
- [38] L. Zhang, B. Liang, H. Zhao, J. Yang, M. Jiao, Y. Liu, Core-shell structured ZnO homojunction for enhanced photocatalysis, *Inorg. Chem. Commun.* 148 (2023), 110281, <https://doi.org/10.1016/j.inoche.2022.110281>.
- [39] G. Yashni, A. Al-Gheethi, R.M.S.R. Mohamed, N.V. Dai-Viet, A.A. Al-Kahtani, M. Al-Sahari, N.J.N. Hazhar, E. Noman, S. Alkhadher, Bio-inspired ZnO NPs synthesized from Citrus sinensis peels extract for Congo red removal from textile wastewater via photocatalysis: optimization, mechanisms, techno-economic analysis, *Chemosphere* 281 (2021), <https://doi.org/10.1016/j.chemosphere.2021.130661>. ARTN 130661.
- [40] V. Srikanth, D.R. Clarke, On the optical band gap of zinc oxide, *J. Appl. Phys.* 83 (1998) 5447–5451, <https://doi.org/10.1063/1.367375>.
- [41] C.Y. Tsay, C.W. Wu, C.M. Lei, F.S. Chen, C.K. Lin, Microstructural and optical properties of Ga-doped ZnO semiconductor thin films prepared by sol-gel process, *Thin Solid Films* 519 (2010) 1516–1520, <https://doi.org/10.1016/j.tsf.2010.08.170>.
- [42] X.X. Zhang, Y.F. Fan, X.M. Tao, K.L. Yick, Fabrication and properties of microcapsules and nanocapsules containing n-octadecane, *Mater. Chem. Phys.* 88 (2004) 300–307, <https://doi.org/10.1016/j.matchemphys.2004.06.043>.
- [43] E.B. Sirota, H.E. King, D.M. Singer, H.H. Shao, Rotator phases of the normal alkanes: an x-ray scattering study, *J. Chem. Phys.* 98 (1993) 5809–5824, <https://doi.org/10.1063/1.464874>.
- [44] P.K. Mukherjee, Phase transitions among the rotator phases of the normal alkanes: a review, *Phys. Rep.* 588 (2015) 1–54, <https://doi.org/10.1016/j.physrep.2015.05.005>.
- [45] D.R. Lide, *CRC Handbook of Chemistry and Physics*, 90th ed., CRC Press, Boca Raton, Florida, USA, 2009.
- [46] J. Korppi-Tommola, R.W. Yip, Solvent effects on the visible absorption spectrum of crystal violet, *Can. J. Chem.* 59 (1981) 191–194, <https://doi.org/10.1139/v81-03>.
- [47] K.-J. Hwang, J.-W. Lee, W.-G. Shim, H.D. Jang, S.-I. Lee, S.-J. Yoo, Adsorption and photocatalysis of nanocrystalline TiO<sub>2</sub> particles prepared by sol-gel method for methylene blue degradation, *Adv. Powder Technol.* 23 (2012) 414–418, <https://doi.org/10.1016/j.apt.2011.05.010>.
- [48] K. Loh, C.C. Gaylarde, M.A. Shirakawa, Photocatalytic activity of ZnO and TiO<sub>2</sub> 'nanoparticles' for use in cement mixes, *Construct. Build. Mater.* 167 (2018) 853–859, <https://doi.org/10.1016/j.conbuildmat.2018.02.103>.
- [49] V.P. Singh, K. Sandeep, H.S. Kushwaha, S. Powar, R. Vaish, Photocatalytic, hydrophobic and antimicrobial characteristics of ZnO nano needle embedded cement composites, *Construct. Build. Mater.* 158 (2018) 285–294, <https://doi.org/10.1016/j.conbuildmat.2017.10.035>.
- [50] B.O. Bica, J.V.S. de Melo, Concrete blocks nano-modified with zinc oxide (ZnO) for photocatalytic paving: performance comparison with titanium dioxide (TiO<sub>2</sub>), *Construct. Build. Mater.* 252 (2020), <https://doi.org/10.1016/j.conbuildmat.2020.119120>.